Thermo X https://doi.org/10.70401/tx.2025.0005

Supplementary information

Anisotropic conductive phase change composites enabled by parallel expanded graphite sheets for solar-thermal energy storage

Heqi Huang, Xinru Yang, Yu Qiu, Xiangkun Elvis Cao, Liu Liu, Chuanchang Li, Xun Chen, Hongjie Yan

Note S1. Uncertainty analysis.

The solar-thermal ($\eta_{\text{s-t}}$) of the PCCs can be calculated using Eq. (S1)[1,2].

$$\eta_{\text{s-t}} = \frac{m \cdot \Delta H}{P \cdot S \cdot \Delta t} \times 100\% \tag{S1}$$

where m is the mass of PCC, g; ΔH is the phase change enthalpy of PCC, $J \cdot g^{-1}$; P is the simulated solar irradiance, $W \cdot m^{-2}$; S is the surface area of PCC, m^2; Δt is the duration of the phase change process, s.

The magnitude of uncertainty reflects the closeness between the measurement result and the true value. In indirect measurements, the uncertainty typically consists of two components: uncertainties from direct measurements and propagation errors. The mathematical foundation of its propagation law lies in the total differential. Assuming the measured physical quantity (N) has a functional relationship with direct measurement quantities (x, y, z, ...) expressed as $N = f(x, y, z, \ldots)$, taking its logarithm followed by total differential yields the following Eq. (S2).

$$\frac{dN}{N} = \frac{\partial \ln f}{\partial x} dx + \frac{\partial \ln f}{\partial y} dy + \frac{\partial \ln f}{\partial z} dz + \cdots \tag{S2}$$

When the uncertainties of directly measured quantities are mutually independent, the uncertainty (σ) can be derived in Eq. (S3). The relative uncertainty can be expressed as Eq. (S4).

$$\sigma = \sqrt{\left(\frac{\partial f}{\partial x}\right)^2 \sigma_x^2 + \left(\frac{\partial f}{\partial y}\right)^2 \sigma_y^2 + \left(\frac{\partial f}{\partial z}\right)^2 \sigma_z^2 + \cdots} \tag{S3}$$

$$\frac{\sigma}{N} = \sqrt{\left(\frac{\partial \ln f}{\partial x}\right)^2 \sigma_x^2 + \left(\frac{\partial \ln f}{\partial y}\right)^2 \sigma_y^2 + \left(\frac{\partial \ln f}{\partial z}\right)^2 \sigma_z^2 + \cdots} \tag{S4}$$

In experiments, the solar-thermal efficiency $\eta_{\text{s-t}}$ of the PCCs is a function of the mass of the sample m (± 0.0001 g), the phase change enthalpy ΔH (± 0.2%), the solar irradiation intensity P (± 3%), the surface area of the sample S (±0.0001 cm^2), the phase change duration Δt (± 5 s). Thus, combining the above equation with these data yields the relative uncertainty (E_η) equation for solar-thermal efficiency $\eta_{\text{s-t}}$ as Eq. (S5)[3,4]. The maximum relative uncertainty (E_η) of solar-thermal efficiency $\eta_{\text{s-t}}$ is 4.44% as shown in **Table S2**, indicating that the experimental results were reliable.

$$E_\eta = \sqrt{\left(\frac{\delta m}{m}\right)^2 + \left(\frac{\delta \Delta H}{\Delta H}\right)^2 + \left(\frac{\delta P}{P}\right)^2 + \left(\frac{\delta S}{S}\right)^2 + \left(\frac{\delta \Delta t}{\Delta t}\right)^2} \tag{S5}$$

Note S2. Calculations of the mass loss rate and solar absorptivity of the PCC.

Shape stability test was conducted using a constant-temperature heating plate, filter paper, and precision balance. The PCC block was placed on filter paper and subjected to constant-temperature heating at 80 °C for 30 min on the heating plate. The mass and morphology of each block were recorded every 5 min. During heating, some PW leaked from the PCC due to solid-liquid phase transition, which was absorbed by the filter paper, resulting in mass loss. The mass loss rate (γ) can be calculated by Eq. (S6)[5].

$$\gamma = \frac{\left(m_t - m_0\right)}{m_0} \times 100\% \tag{S6}$$

where m_t is the mass of the PCC block at a time point during the heating process, g; m_0 is the initial mass of the PCC block, g.

The solar absorptivity (A) of the upper surface of each sample within the main solar spectrum (0.3-2.5 μm) can be calculated using Eq. (S7) based on its measured spectral absorptivity[6].

$$A = \frac{\int_{0.3\mu\text{m}}^{2.5\mu\text{m}} A(\Lambda) I_{\text{AM1.5}}(\Lambda) d\Lambda}{\int_{0.3\mu\text{m}}^{2.5\mu\text{m}} I_{\text{AM1.5}}(\Lambda) d\Lambda} \tag{S7}$$

where Λ is wavelength, μm; $A(\Lambda)$ is the spectral absorptivity of the sample surface; $I_{\text{AM1.5}}(\Lambda)$ is the spectral irradiance of the AM1.5 reference solar spectral irradiance[7], $W \cdot m^{-2} \cdot \mu m^{-1}$.

Note S3. Parallel and series heat conduction models.

The volumetric proportion of EG (φ_{v}) in the PCC can be calculated from its mass proportion (φ_{wt}) through Eq. (S8).

$$\varphi_{\text{v}} = \frac{\dfrac{\varphi_{\text{wt}}}{\rho_{\text{EG}}}}{\dfrac{\varphi_{\text{wt}}}{\rho_{\text{EG}}} + \dfrac{1 - \varphi_{\text{wt}}}{\rho_{\text{PW-OBC}}}} \tag{S8}$$

where ρ_{EG} and $\rho_{\text{PW-OBC}}$ are the densities of the EG and PW-OBC sheets, respectively.

To define the upper and lower bounds of thermal resistance along the heat flow path, parallel and series thermal conduction models were established (**Figure S4**). These bounds directly determine the minimum and maximum achievable heat transfer rates. The lengthwise (R_{par}) and transverse (R_{ser}) thermal resistances are given in Eq. (S9) and Eq. (S10), respectively.

$$\frac{1}{R_{\text{par}}} = \frac{\varphi_{\text{v}}}{R_{\text{EG}}} + \frac{\left(1 - \varphi_{\text{v}}\right)}{R_{\text{PW-OBC}}} \tag{S9}$$

$$R_{\text{ser}} = \varphi_{\text{v}} R_{\text{EG}} + (1 - \varphi_{\text{v}}) R_{\text{PW-OBC}} \tag{S10}$$

Where R_{EG} and $R_{\text{PW-OBC}}$ are the thermal resistances of the EG sheet and PW-OBC mixture, respectively.

The ratio $\lambda_{\text{L}}/\lambda_{\text{T}}$ represents the thermal conductive anisotropy, where λ_{T} and λ_{L} denote the transverse and longitudinal conductivities, respectively. Based on the series and parallel heat conduction models, its expression can be given by Eq. (S11).

$$\frac{\lambda_{\text{L}}}{\lambda_{\text{T}}} = \left(\frac{\lambda_{\text{PW-OBC}}}{\lambda_{\text{EG}}} + \frac{\lambda_{\text{EG}}}{\lambda_{\text{PW-OBC}}} \right) \varphi_{\text{v}} (1 - \varphi_{\text{v}}) + (1 - \varphi_{\text{v}})^2 + \varphi_{\text{v}}^2 \tag{S11}$$

where λ_{EG} and $\lambda_{\text{PW-OBC}}$ refer to the thermal conductivities of the EG and PW-OBC sheets, respectively.

Supporting Figures.

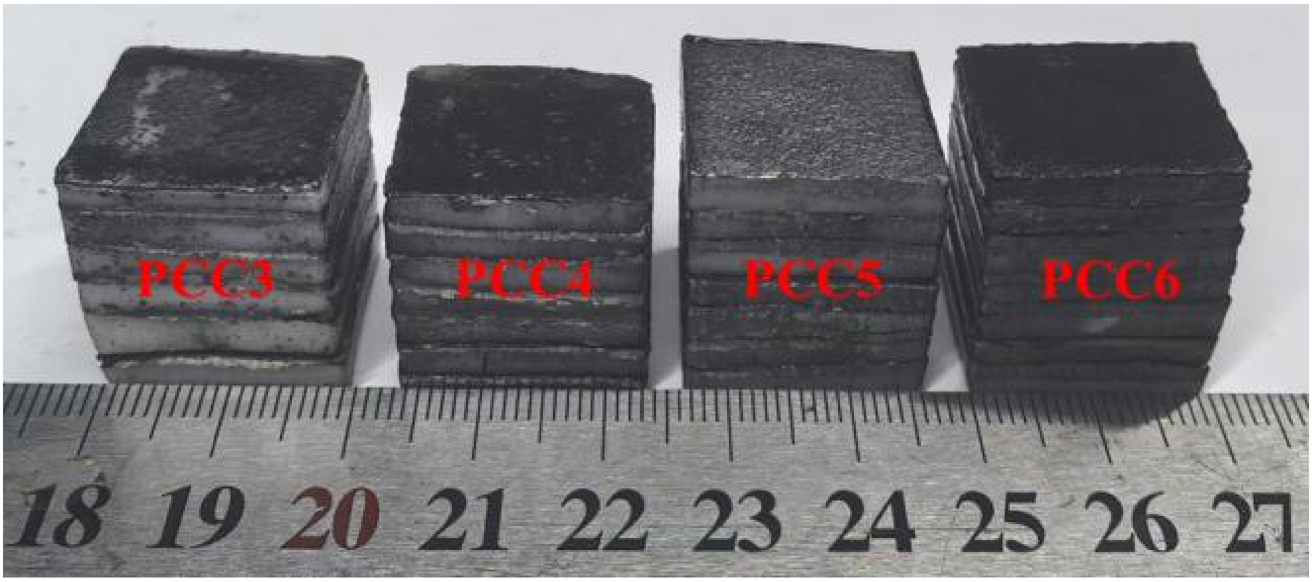

Figure S1. Photographs of PCC3-PCC6 samples with varying expanded graphite (EG) proportion.

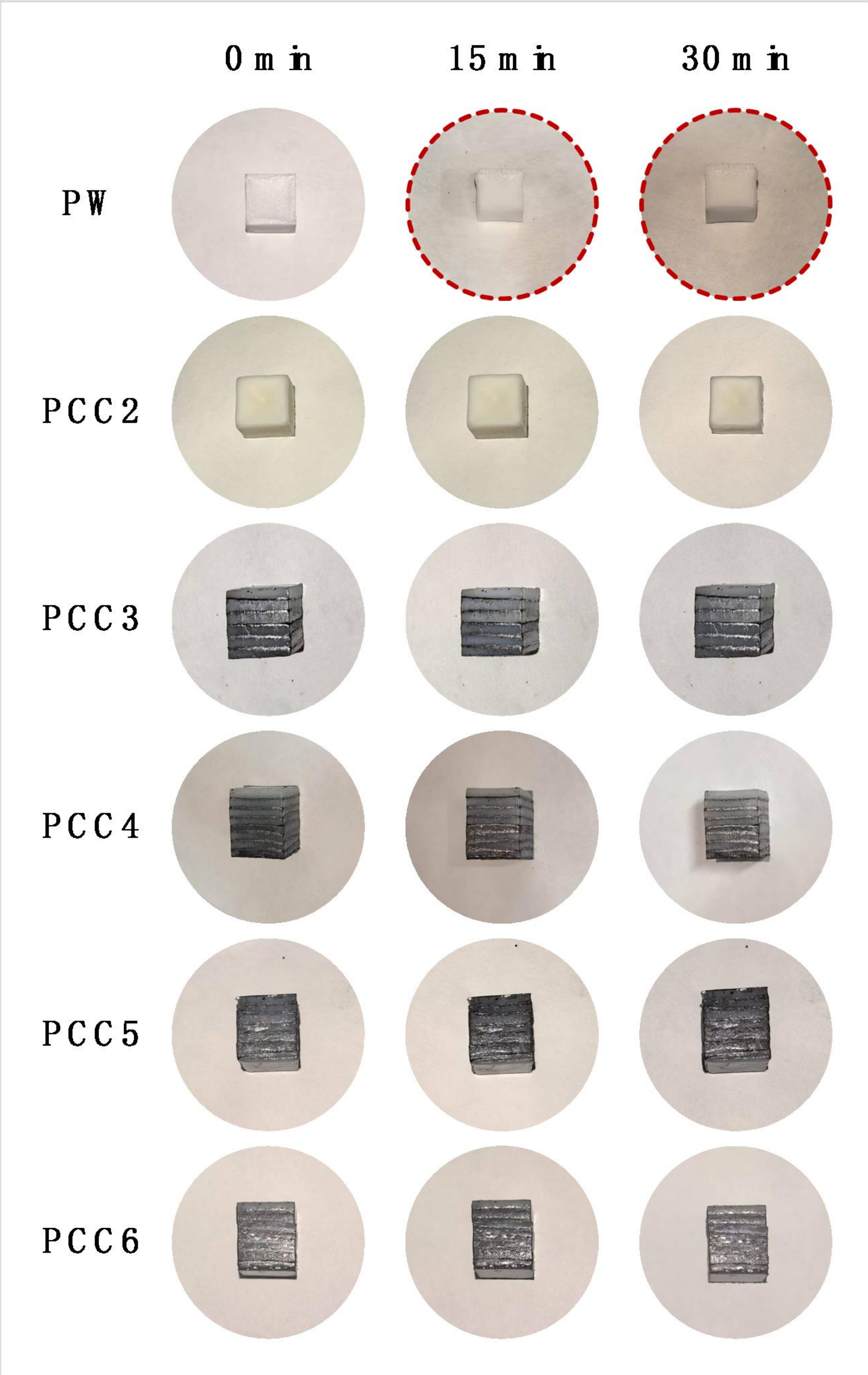

Figure S2. Time-lapse photos of PW and PCC samples with dimensions 20 × 20 × 20 mm^3.

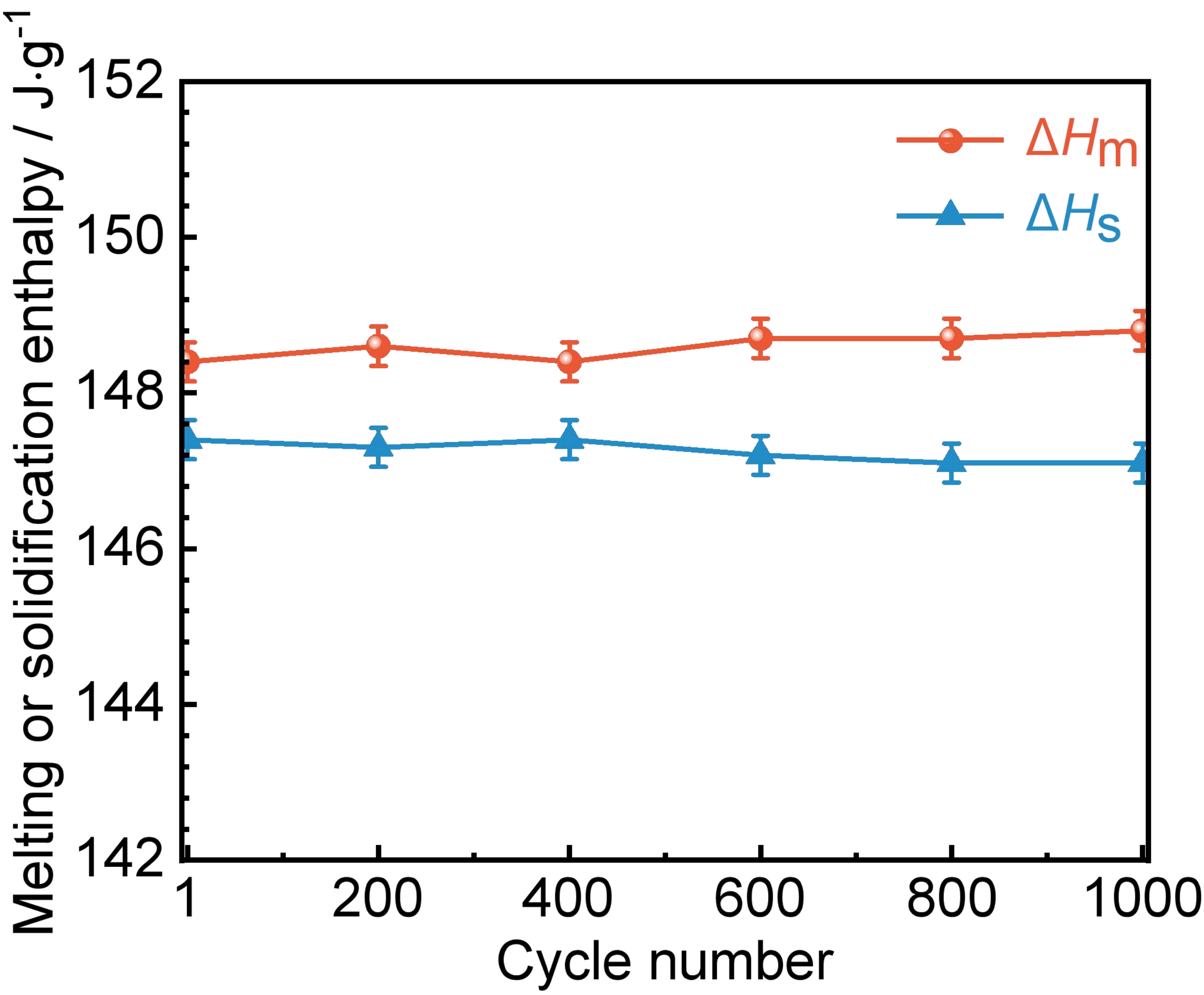

Figure S3. The Measured melting (ΔH_m) and solidification (ΔH_s) enthalpies of the PCC6 under 1,000 heating/cooling cycles within 20 °C-90 °C.

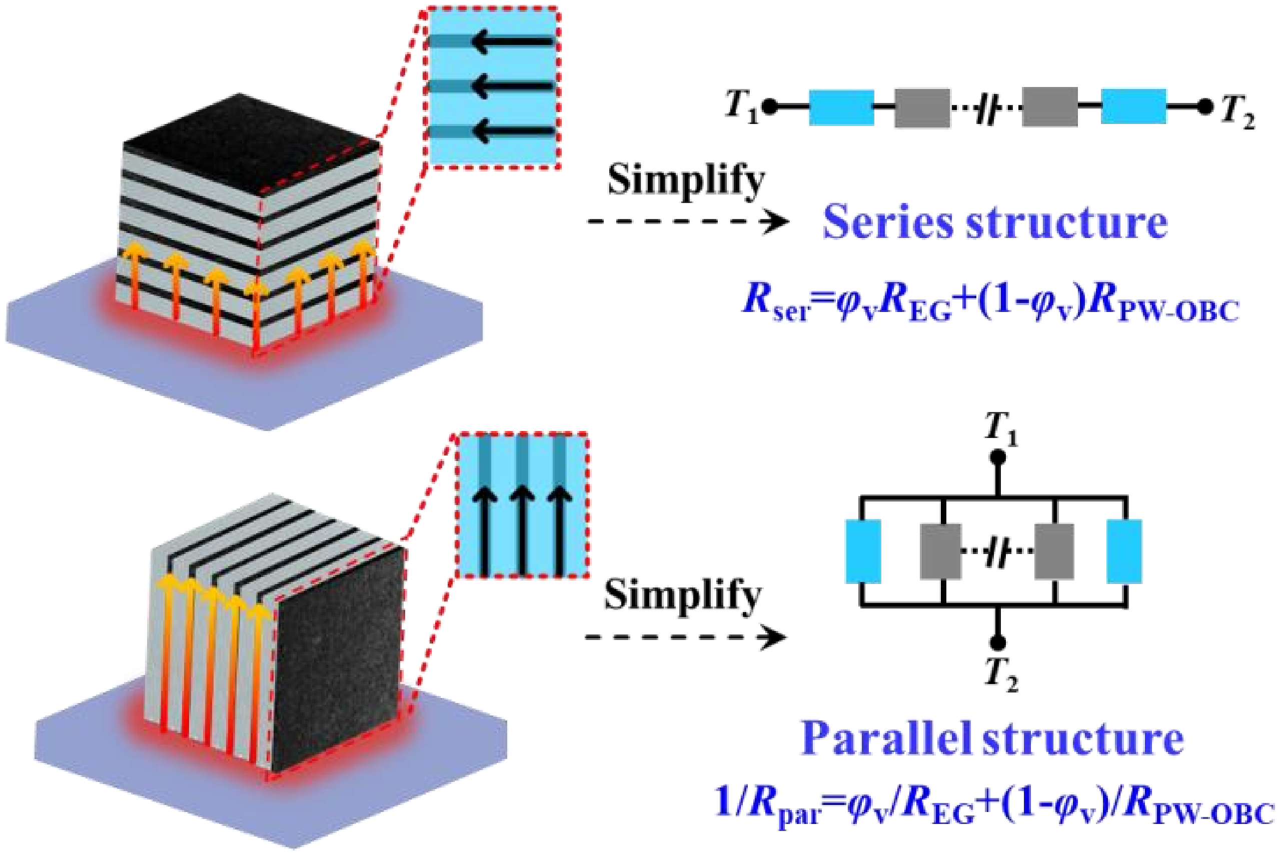

Figure S4. Schematic diagrams of the PCC's series and parallel thermal models.

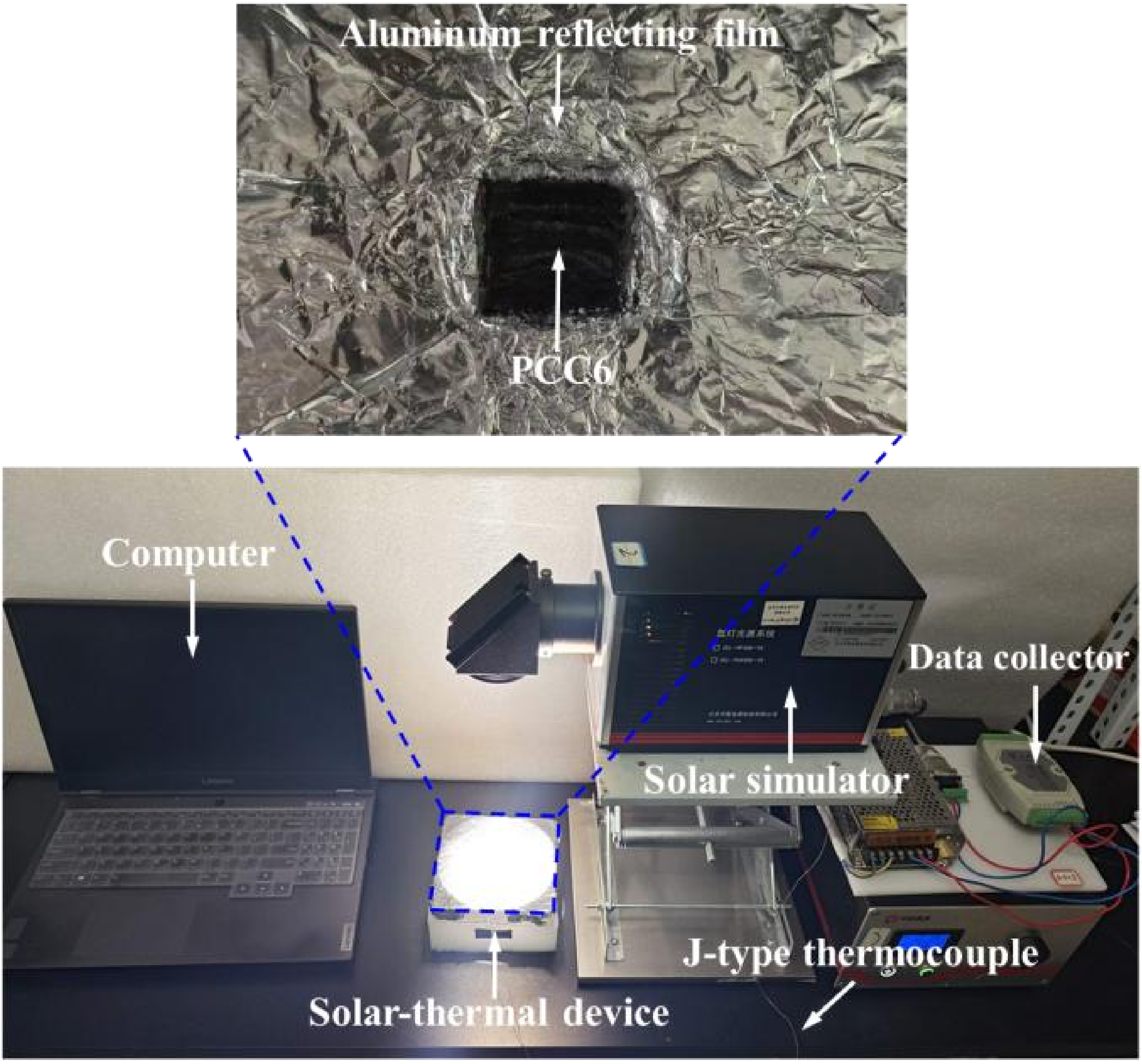

Figure S5. Photos showing the PCC-based direct solar-thermal energy storage device (left) and the solar-thermal testing setup (right).

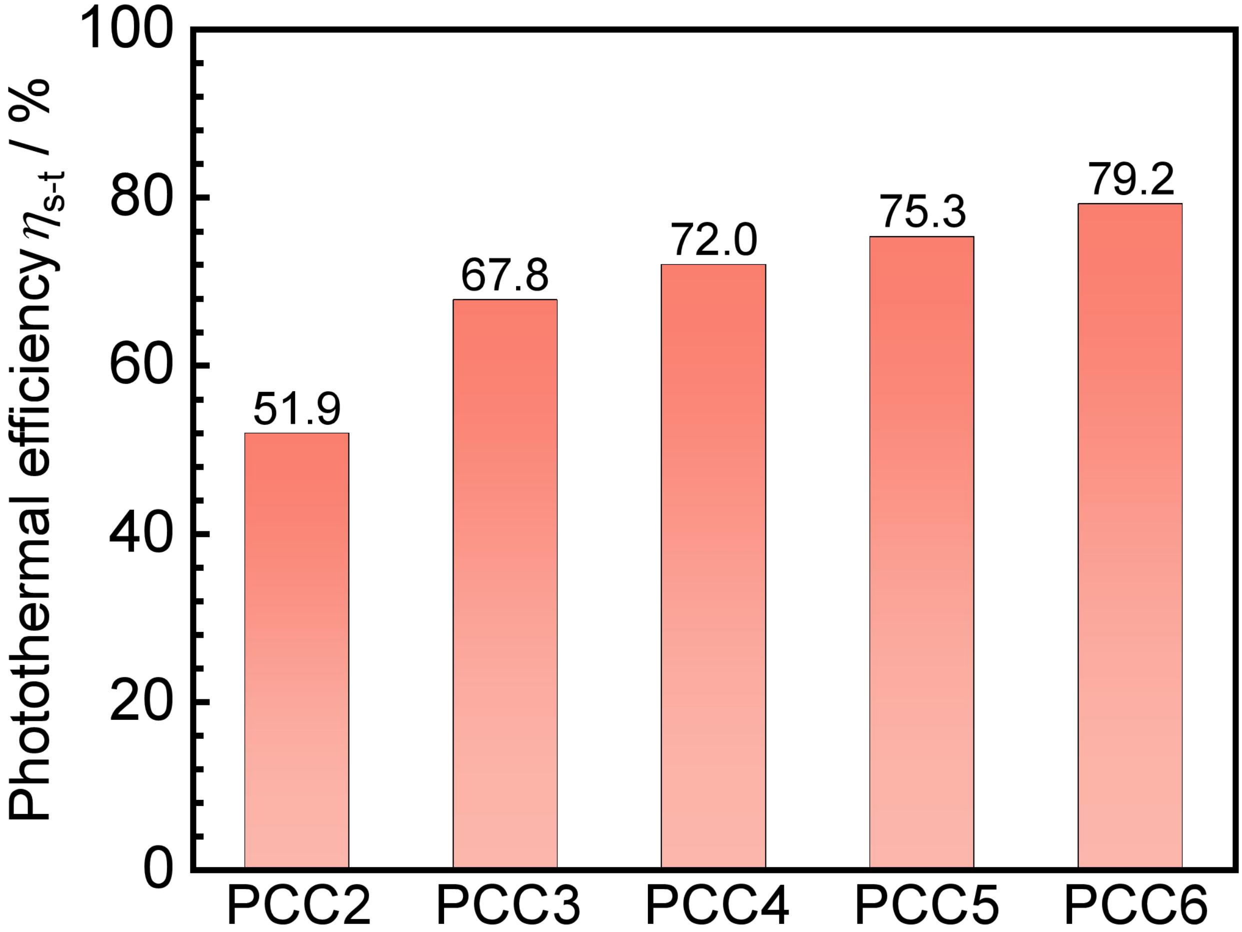

Figure S6. Solar-thermal efficiencies of the PCCs under 1 sun.

Supporting Tables.

Table S1. Thermal conductivities of present PCCs and some recently open-published PCCs.

λ_L/W·m^{-1}·K^{-1}	λ_T/W·m^{-1}·K^{-1}	Thermal conductive Anisotropy λ_L/λ_T	Reference
5.63	0.77	7.31	[3]
5.84	1.34	4.36	[6]
10.55	2.60	4.06	[8]
6.75	2.92	2.31	[9]
1.2453	0.1933	6.44	[10]
0.8	0.5	1.6	[11]
21.3	8.29	2.57	[12]
15.5	10.1	1.53	[13]
6.31	2.95	2.14	[14]
1.84	1.38	1.33	[15]
8.87	2.68	3.31	[16]
1.73	0.62	2.79	[17]
4.54	**0.49**	**9.27**	**This work**

Table S2. Results of uncertainty analysis.

Sample	m (g)	ΔH (J·g^{-1})	P (kW·m^{-2})	S (cm^2)	Δt (s)	E_η (%)
PCC2	1.3343	189.5	1.0	4.0	1,217	3.03
PCC3	1.2279	180.1	1.0	4.0	815	3.07
PCC4	1.2770	169.7	1.0	4.0	752	3.08
PCC5	1.2091	161.0	1.0	4.0	646	3.10
PCC6	1.1935	148.4	1.0	4.0	559	3.14
$PCC6_L$ with glass	1.1935	148.4	1.0	4.0	556	3.14
$PCC6_H$	1.3155	148.4	1.0	4.0	737	3.08
$PCC6_L$	1.1935	148.4	1.5	4.0	353	3.32

$PCC6_L$ with glass	1.1935	148.4	1.5	4.0	351	3.33
$PCC6_H$	1.3155	148.4	1.5	4.0	453	3.20
$PCC6_L$	1.1935	148.4	2.0	4.0	247	3.62
$PCC6_L$ with glass	1.1935	148.4	2.0	4.0	248	3.62
$PCC6_H$	1.3155	148.4	2.0	4.0	320	3.39
$PCC6_L$	1.1935	148.4	2.5	4.0	189	4.00
$PCC6_L$ with glass	1.1935	148.4	2.5	4.0	191	3.99
$PCC6_H$	1.3155	148.4	2.5	4.0	250	3.61
$PCC6_L$	1.1935	148.4	3.0	4.0	153	4.44
$PCC6_L$ with glass	1.1935	148.4	3.0	4.0	156	4.39
$PCC6_H$	1.3155	148.4	3.0	4.0	200	3.91

Table S3. Mass values of PW and different PCCs at different time points.

Time/min	m_{PCC1}/g	m_{PCC2}/g	m_{PCC3}/g	m_{PCC4}/g	m_{PCC6}/g
0	7.298	7.338	7.363	7.619	8.128
5	7.286	7.333	7.362	7.617	8.124
10	7.227	7.330	7.358	7.614	8.122
15	7.214	7.329	7.357	7.612	8.119
20	7.108	7.323	7.354	7.608	8.116
25	7.106	7.323	7.351	7.607	8.113
30	7.104	7.322	7.350	7.604	8.112

Table S4. Phase change temperatures and enthalpies of the PW and PCCs.

Sample	PW content/wt.%	T_m/°C	ΔH_m , ΔH_{pre}/J·g^{-1}	T_s/°C	ΔH_s , ΔH_{pre}/J·g^{-1}
PW	100.00	52.9	249.9, 249.9	46.3	248.9, 248.9
PCC2	75.00	53.7	189.5, 187.4	37.6	187.9, 186.7
PCC3	71.25	53.7	180.1, 178.1	38.9	177.6, 177.3
PCC4	67.50	51.2	169.7, 168.7	41.4	167.2, 168.0
PCC5	63.75	53.2	161.0, 159.3	40.4	160.3, 158.7
PCC6	60.00	52.1	148.4, 149.9	40.6	147.4, 149.3

Table S5. Thermal conductivity enhancing factors (α_λ) in this work and existing studies.

Base material	Filler	φ_{wt}/%	λ_{PCM}/W·m^{-1}·K^{-1}	λ_{PCC}/W·m^{-1}·K^{-1}	α_λ/%	Reference
PW/OBC	CFs	10	0.21	2.23	106.19	[3]
OC	CF/CNT	11	0.26	1.31	45.80	[18]
Erythritol	SCFs	10	0.77	3.91	50.78	[19]
SAT	EPCu	5.7	0.59	3.22	95.75	[20]
SA	rGO	3	0.41	1.25	101.63	[21]
$Mg(NO_3)_2{\cdot}6H_2O$/ g-C_3N_4	GS	10	0.38	2.43	63.95	[22]
PEG	PVA-rGO	3.1	0.221	0.348	50.80	[23]
PW	SCA	13	0.23	0.43	14.38	[24]
mE/2DNH	EG	20	0.714	12.36	86.55	[25]
C14/PCL	EG	15	0.224	3.702	110.18	[26]
PA/PE	EG	10	0.25	1.9955	79.82	[27]
PW	HPC2.0	16.04	0.27	0.33	7.62	[28]

PA	CFs	20	0.23	5.21	113.26	[14]
Paraffin wax/ Olefin block copolymer	**EG**	**0**	**0.18**	-	-	**This work**
		5	**0.18**	**1.20**	**135.33**	**This work**
		10	**0.18**	**2.28**	**126.67**	**This work**
		15	**0.18**	**3.24**	**120.00**	**This work**
		20	**0.18**	**4.54**	**126.11**	**This work**

Table S6. The solar-thermal energy conversion and storage performance of the $PCC6_L$.

Solar irradiation P/W·m^{-2}	1,000	1,500	2,000	2,500	3,000
Phase change duration $\triangle t$/s	559	353	247	189	153
Surface area S/cm^2	4.0				
Mass m/g	1.19				
Input energy/J	223.6	211.8	197.6	189.0	183.6
Stored energy/J	177.1				
Solar-thermal efficiency $\eta_{s\text{-}t}$/%	79.2	83.6	89.6	93.7	96.5

Table S7. The solar-thermal energy harvesting performance of the $PCC6_T$.

Solar irradiation P/W·m^{-2}	1,000	1,500	2,000	2,500	3,000
Phase change duration $\triangle t$/s	737	453	320	250	200
Surface area S/cm^2	4.0				
Mass m/g	1.32				
Input energy/J	294.8	271.8	256.0	250.0	240.0
Stored energy/J	195.2				
Solar-thermal efficiency $\eta_{s\text{-}t}$/%	66.2	71.8	76.3	78.1	81.3

Table S8. The solar-thermal energy harvesting performance of the PCC6$_L$ with glass.

Solar irradiation P/W·m^{-2}	1,000	1,500	2,000	2,500	3,000
Phase change duration △t/s	556	351	248	191	156
Surface area S/cm^2	4.0				
Mass m/g	1.19				
Input energy/J	222.4	210.6	198.4	191.0	187.2
Stored energy/J	177.1				
Solar-thermal efficiency $\eta_{s\text{-}t}$/%	79.6	84.1	89.3	92.7	94.6

Table S9. Solar-thermal efficiencies of present PCCs and some open-published PCCs.

PCC	Phase change temperature/°C	Solar irradiation /sun	Solar-thermal efficiency $\eta_{s\text{-}t}$/%	Reference
TME/EG	83.1	3.0	69.49	[29]
OC/CF/CNT	58.21	3.0	82.6	[18]
SAT/EPCu	50.89	1.2	80.81	[20]
Ag-MWCNTs/PW @CNS	60.91	1.2	73.1	[30]
PEG/PVA-GO	59.1	1.2	82.3	[23]
LA/GA	43.31	1.0	74.6	[31]
CNT/PDA@ SiO_2-MEPCM	37.3	3.0	90.1	[32]
mE/2DHN/EG	119.57	3.0	75.72	[25]
Erythritol-PAAS/GO	119	1.0	69.2	[8]
HPC2.0/PW	52.36	2.5	38.0	[28]
HPC2.0/PW	52.36	3.0	89.0	[28]
PW/OBC/CFs	56	1.0	79.17	[3]
PW-OBC/EG	**52.1**	**1.0**	**79.2**	**This work**
PW-OBC/EG	**52.1**	**1.5**	**83.6**	**This work**
PW-OBC/EG	**52.1**	**2.0**	**89.6**	**This work**
PW-OBC/EG	**52.1**	**2.5**	**93.7**	**This work**
PW-OBC/EG	**52.1**	**3.0**	**96.5**	**This work**

Noting: TME-Trimethylolethane, EG-Expanded graphite, OC-octadecanol, CF-Carbon foam, CNT-Carbon nanotube, SAT- Sodium acetate trihydrate, EPCu-Modified expanded graphite, Ag-MWCNTs/PW@CNS-Silver-decorated carboxyl multi-wall carbon nanotubes/paraffin wax

@Carbon nanotube sponge, PEG-Poly ethylene glycol, PVA-Polyvinyl alcohol, GO-Graphene oxide, LA-Lauric acid, GA-Graphene aerogel, PDA-Polydopamine,SiO_2-MEPCM-Silica hierarchical shell, mE-Meso-erythritol, 2DHN-two-dimensional heterogeneous nanohybrids, PAAS-Polyamic acid salt, HPC-Hierarchical porous carbon, PW-Paraffin wax, OBC- Olefin block copolymer, CFs-Carbon fibers.

References

1.Hu Y, Huang Y, Liu X, Fu M, Luo S, Li Y, et al. Synergistically enhanced NF/CNTs@ PDA/PEG composite phase change materials for high-efficiency solar-thermal energy storage and conversion. Sol Energy Mater Sol Cells. 2025;290:113714. [DOI: 10.1016/j.solmat.2025.113714]

2.Wang C, Dong W, Li A, Atinafu DG, Wang G, Lu Y. The reinforced photothermal effect of conjugated dye/graphene oxide-based phase change materials: Fluorescence resonance energy transfer and applications in solar-thermal energy storage. Chem Eng J. 2022;428(24):130605. [DOI: 10.1016/j.cej.2021.130605]

3.Zhang P, Qiu Y, Ye C, Li Q. Anisotropically conductive phase change composites enabled by aligned continuous carbon fibers for full-spectrum solar thermal energy harvesting. Chem Eng J. 2023;461:141940. [DOI: 10.1016/j.cej.2023.141940]

4.Aftab W, Mahmood A, Guo W, Yousaf M, Tabassum H, Huang X, et al. Polyurethane-based flexible and conductive phase change composites for energy conversion and storage. Energy Storage Mater. 2019;20:401-409. [DOI: 10.1016/j.ensm.2018.10.014]

5.Wu W, Wu W, Wang S. Form-stable and thermally induced flexible composite phase change material for thermal energy storage and thermal management applications. Appl Energy. 2019;236:10-21. [DOI: 10.1016/j.apenergy.2018.11.071]

6.Zhang P, Wang Y, Qiu Y, Yan H, Wang Z, Li Q. Novel composite phase change materials supported by oriented carbon fibers for solar thermal energy conversion and storage. Appl Energy. 2024;358:122546. [DOI: 10.1016/j.apenergy.2023.122546]

7.Materials ASfTa. Standard tables for reference solar spectral irradiances: Direct normal and hemispherical on 37° tilted surface: ASTM International; 2003. [DOI: 10.1520/G0173-23]

8.Zhang Q, Dai Z, Gu B, Zhao D. Thermally conductive phase change composites for efficient medium-temperature solar thermal storage. J Energy Storage. 2025;113:115687. [DOI: 10.1016/j.est.2025.115687]

9.Li W, Yang T, Chen L, Shi J, Zhang T, Zeng C, et al. Thermal management study of cylindrical battery using novel thermally conductive anisotropic flexible phase change material. Case Stud Therm Eng. 2025;73:106508. [DOI: 10.1016/j.csite.2025.106508]

10.Huang J, Sun X, Liang B, Li Z, Zheng D, Yang B, et al. Preparation and properties of phase-change materials with enhanced radial thermal conductivities based on anisotropic graphene aerogels. RSC Adv. 2024;14:2763-2769. [DOI: 10.1039/d3ra06835h]
11.Li C, Zhang D, Ren W. Phase change materials composite based on hybrid aerogel with anisotropic microstructure. Materials. 2021;14:777.
12.Dai Z, Gao Y, Wang C, Wu D, Jiang Z, She X, et al. Oriented high thermal conductivity solid–solid phase change materials for mid-temperature solar-thermal energy storage. ACS Appl Mater Interfaces. 2023;15(22):26863-26871. [DOI: 10.1021/acsami.3c04429]
13.Shu C, Zhao H-Y, Zhao S, Deng W, Min P, Lu X-H, et al. Highly thermally conductive phase change composites with anisotropic graphene/cellulose nanofiber hybrid aerogels for efficient temperature regulation and solar-thermal-electric energy conversion applications. Compos Part B Eng. 2023;248(6):110367. [DOI: 10.1016/j.compositesb.2022.110367]
14.Hu J, Yao Z, Chen A, Xiao C, Zhang G, Yang X. High thermal-conductive phase change material by carbon fiber orientation for thermal management and energy conversion application. Appl Therm Eng. 2025;265(5):125566. [DOI: 10.1016/j.applthermaleng.2025.125566]
15.Cao H, Li S-Z, Yang J, Liu Z-Y, Bai L, Yang W. Thermally conductive magnetic composite phase change materials for anisotropic photo/magnetic-to-thermal energy conversion. ACS Appl Mater Interfaces. 2023;15(48):55723-55733. [DOI: 10.1021/acsami.3c12302]
16.Min P, Liu J, Li X, An F, Liu P, Shen Y, et al. Thermally conductive phase change composites featuring anisotropic graphene aerogels for real-time and fast-charging solar-thermal energy conversion. Adv Funct Mater. 2018;28(51):1805365. [DOI: 10.1002/adfm.201805365]
17.Sheng N, Rao Z, Zhu C, Habazaki H. Honeycomb carbon fibers strengthened composite phase change materials for superior thermal energy storage. Appl Therm Eng. 2020;164:114493. [DOI: 10.1016/j.applthermaleng.2019.114493]
18.Li SY, Yan T, Huo YJ, Pan WG. Carbon nanotube/carbon foam thermal-bridge enhancing solar energy conversion and storage of phase change materials. Mater Today Sustain. 2024;28:100986. [DOI: 10.1016/j.mtsust.2024.100986]
19.Zhang Q, Luo Z, Guo Q, Wu G. Preparation and thermal properties of short carbon fibers/erythritol phase change materials. Energy Convers Manage. 2017;136:220-228. [DOI: 10.1016/j.enconman.2017.01.023]
20.Liu P, Wang C, Cheng X, Wang S, Wang Z. Preparation and photothermal investigation of PDA and CuNPs coupled modified expanded graphite with sodium acetate trihydrate composite phase change materials. Sol Energy. 2025;293:113478. [DOI: 10.1016/j.solener.2025.113478]

21.Liu L, Zheng K, Yan Y, Cai Z, Lin S, Hu X. Graphene Aerogels Enhanced Phase Change Materials prepared by one-pot method with high thermal conductivity and large latent energy storage. Sol Energy Mater Sol Cells. 2018;185:487-93. [DOI: 10.1016/j.solmat.2018.06.005]
22.Zhang W, Ling Z, Fang X, Zhang Z. Anisotropically conductive $Mg(NO_3)_2 \cdot 6H_2O$/g-C_3N_4-graphite sheet phase change material for enhanced photo-thermal storage. Chem Eng J. 2022;430(7):132997. [DOI: 10.1016/j.cej.2021.132997]
23.Luo L, Luo W, Chen W, Hu X, Ma Y, Xiao S, et al. Form-stable phase change materials based on graphene-doped PVA aerogel achieving effective solar energy photothermal conversion and storage. Sol Energy. 2023;255(2):146-156. [DOI: 10.1016/j.solener.2023.03.037]
24.Wei Y, Li J, Sun F, Wu J, Zhao L. Leakage-proof phase change composites supported by biomass carbon aerogels from succulents. Green Chem. 2018;20(8):1858-1865. [DOI: 10.1039/c7gc03595k]
25.Pan C, He P, Chen N, Wu J, Shi E, Wang A, et al. Highly thermally conductive composite phase-change materials doped with two-dimensional heterogeneous nanohybrids for photo/electro-thermal energy storage. J Energy Storage. 2023;57:106225. [DOI: 10.1016/j.est.2022.106225]
26.Zeng C, Shu Q, Li W, Qin X. Enhancing thermal performance of low-temperature phase change materials based on tetradecane. Energy Build. 2025;345:116112. [DOI: 10.1016/j.enbuild.2025.116112]
27.Xu C, Shen L, Wen Z, Zhou R, Hao M, Jiang J. Synergistic enhancement of shape stability and thermal properties of phase change materials by MOF/EG composite carriers. Mater Lett. 2025;395:138674. [DOI: 10.1016/j.matlet.2025.138674]
28.Sun K, Kou Y, Zhang Y, Liu T, Shi Q. Photo-triggered hierarchical porous carbon-based composite phase-change materials with superior thermal energy conversion capacity. ACS Sustain Chem Eng. 2020;8(8):3445-3453. [DOI: 10.1021/acssuschemeng.9b07659]
29.Zhao Y, Zhang P, Qiu Y, Li Q, Yan H, Wang Z, et al. Highly conductive solid-solid phase change composites and devices enhanced by aligned graphite networks for solar/electro-thermal energy storage. DeCarbon. 2024;5:100051. [DOI: 10.1016/j.decarb.2024.100051]
30.Zhou L, Wang X, Wu Q, Ni Z, Zhou K, Wen C, et al. Carbon nanotube sponge encapsulated Ag-MWCNTs/PW composite phase change materials with enhanced thermal conductivity, high solar-/electric-thermal energy conversion and storage. J Energy Storage. 2024;84(1):110925. [DOI: 10.1016/j.est.2024.110925]
31.Mu B, Li M. Synthesis of novel form-stable composite phase change materials with modified graphene aerogel for solar energy conversion and storage. Sol Energy Mater Sol Cells. 2019;191(4):466-475. [DOI: 10.1016/j.solmat.2018.11.025]

32.Sun Z, Shi T, Wang Y, Li J, Liu H, Wang X. Hierarchical microencapsulation of phase change material with carbon-nanotubes/polydopamine/silica shell for synergistic enhancement of solar photothermal conversion and storage. Sol Energy Mater Sol Cells. 2022;236:111539. [DOI: 10.1016/j.solmat.2021.111539]